

## Power Stabilization System with Unique Pumped Storage to Stabilize Momentarily Fluctuating Power from Renewable Resources (Counter-Rotating Type Pump-Turbine Unit Operated at Turbine Mode)

Jin-Hyuk Kim<sup>1</sup>, Risa Kasahara<sup>2</sup>, Toru Miyaji<sup>2</sup>, Toshiaki Kanemoto<sup>3</sup> and Young-Seok Choi<sup>1</sup>

<sup>1</sup> Green Energy System Technology Center  
Korea Institute of Industrial Technology

89 Yangdaegiro-gil, Ippang-myeon, Seobuk-gu, Cheonan-si, Chungcheongnam-do, 331-822 (Korea)  
Phone/Fax number: +82 41 5898447/+82 41 5898330, e-mail: [jinhyuk@kitech.re.kr](mailto:jinhyuk@kitech.re.kr), [yschoi@kitech.re.kr](mailto:yschoi@kitech.re.kr)

<sup>2</sup> Graduate School of Engineering  
Kyushu Institute of Technology  
Sensui 1-1, Tobata, Kitakyushu, 804-8550 Fukuoka (Japan)  
e-mail: [m344113r@tobata.isc.kyutech.ac.jp](mailto:m344113r@tobata.isc.kyutech.ac.jp), [n344154t@tobata.isc.kyutech.ac.jp](mailto:n344154t@tobata.isc.kyutech.ac.jp)

<sup>3</sup> Faculty of Engineering  
Kyushu Institute of Technology  
Sensui 1-1, Tobata, Kitakyushu, 804-8550 Fukuoka (Japan)  
Phone/Fax number: +81 93 8843418, e-mail: [kanemoto@mech.kyutech.ac.jp](mailto:kanemoto@mech.kyutech.ac.jp)

**Abstract.** This serial research proposes the hybrid power stabilization system with the counter-rotating type pump-turbine unit, to stabilize momentarily fluctuating power from renewable energy resources. In this paper, the experiments are verified that this type pump-turbine unit is reasonably effective to stabilize momentarily/instantaneously the unstably fluctuating power from renewable energy resources. Furthermore, an optimization for improving the hydrodynamic performance at turbine mode of this pump-turbine unit is carried out by using numerical analysis based on three-dimensional Reynolds-averaged Navier-Stokes equations. As a result, the optimization yielded a maximum increase in efficiency of 2.68% at the best efficiency point compared to a reference design. Detailed internal flow fields between the reference and optimum designs are analyzed and discussed in this work.

### Key words

Power stabilization system, counter-rotating type pump-turbine unit, wind turbine unit, turbine mode, optimization.

### 1. Introduction

In order to extract the renewable energy resources from nature such as hydro, wind, solar, ocean, and so on, there has been increasing interest in the advanced technologies for the high-performance design of renewable turbomachines in the past several years. However, it is difficult to supply unceasingly the stable power from such resources, owing to unforeseen circumstances by an abrupt change in the weather. Hence, the power stabilization system should be certainly constructed to solve the aforementioned problems, with various ideas. Recently, Kanemoto and his colleagues [1~2] have proposed the

newly power stabilization system with the counter-rotating type pump-turbine unit for the unique pumped storage. They demonstrated that this system can instantaneously stabilize the output from the wind power station with the additional help of the counter-rotating type pump-turbine unit for the unique pumped storage. This advanced technology is available for not only the wind power but also the foregoing all renewable energies.

Many studies have lately carried out to improve the hydrodynamic performance of counter-rotating type pump units or pump-turbine units using a range of experimental and computational methods. The advantages of this counter-rotating technique were demonstrated already by many researchers. Add to this Kanemoto et al. [3] have invented the unique double rotational armatures coupled with the counter-rotating type impellers or runners, to suppress the unstable performance and cavitation in the entire operation region. They have called such this features 'smart control' for thirteen years [4].

This work proposes the hybrid power stabilization system with the counter-rotating type pump-turbine unit, and verifies the fruitful performances at both the pumping and turbine modes of a counter-rotating type pump-turbine unit, to stabilize momentarily fluctuating power from renewable energy resources. Moreover, this study presents an optimization procedure for the high performance design at turbine mode of a counter-rotating type pump-turbine unit based on three-dimensional Reynolds-averaged Navier-Stokes (RANS) analyses.

## 2. Power Stabilization System with Pumped Storage

As the wind power station is the most distinctive for the instability and fluctuation among the renewable energy resources, it was applied as an example for the power stabilization system. Figure 1 shows the output from the intelligent wind power unit in house works, and its output was averaged every one minute as shown in Fig. 2, where the average output is arbitrarily 16,000 times as high as one in Fig. 1. It is assumed conveniently, here, that the wind power station should provide the constant power  $P_G$  of 1 MW for the grid system. The output from the wind power unit provides not only the constant power  $P_G$  for the grid system but also the surplus power for the pump-turbine unit at the pumping mode, while the wind velocity is faster than that giving  $P_G$ . On the contrary, the hydroelectric power, namely the turbine mode of this unit, compensates the constant  $P_G$  in uniting with the output from the wind power unit, while the wind velocity is slower than that giving  $P_G$ . Then the pumping mode or the turbine mode is instantaneously determined every one minute in Fig. 2, judging the output from the wind power unit, where the final target of this work is to make average time short as possible.

Figure 3 shows the diagram of the power stabilization system with the counter-rotating type pump-turbine unit. The system is mainly composed of the electric accumulator with the minimal capacity, the power control device, and counter-rotating type pump-turbine unit. The output from the wind turbine connects directly to the electric accumulator, and the power control device detects that the output is higher or lower than  $P_G$ . The power control device demands the electric accumulator not only to provide the constant power  $P_G$  for grid system but also to operate the pump-turbine unit at the pumping mode by the surplus power, while the wind velocity is faster than that giving  $P_G$ , as shown in Fig 3. That is, the surplus output is stored, at once, as the potential energy by the pumping mode. On the contrary, as shown in Fig 3, the power control device demands the pump-turbine unit to operate at the turbine mode converting from the stored potential energy to the hydroelectric output, so as to take  $P_G$  with accompanying the shortage output from the wind power unit.

Figure 4 shows the water volume of the upper and the lower storage tanks in the power stabilization system. Moreover, Fig. 5 shows the integrated wattmeter in the accumulator, where the pumping/turbine head is 15 m, the input is 625 kW at the pumping mode, and the hydroelectric output is adjusted to guarantee  $P_G$  in response to the output from the wind power unit. The electrical accumulator requires the capacity up to 24 kWh as shown in Fig. 5(a), while the power stabilization system operates in Fig. 4. The capacity 24 kWh is 1-8th of the capacity of the electrical accumulator installed traditionally in the wind power station without the proposed stabilization system, as confirmed in Fig. 5. To put the above stabilization system into the practical use, the pump-turbine unit suitable for above operations should be prepared.

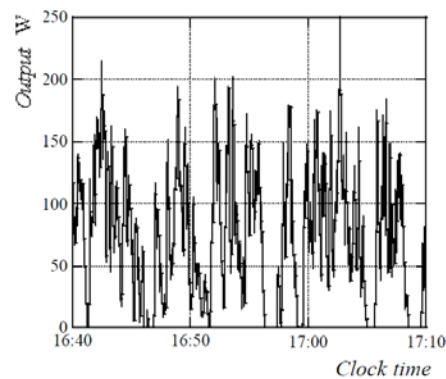


Fig. 1. Output from the wind power unit in house.

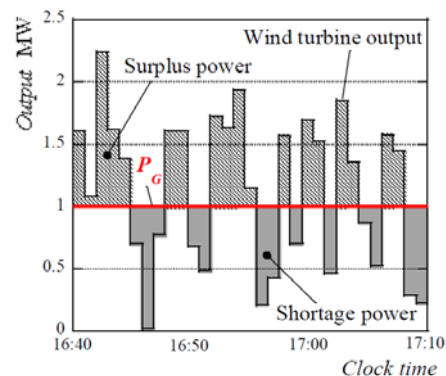


Fig. 2. Result of output averaged every 1 minute.

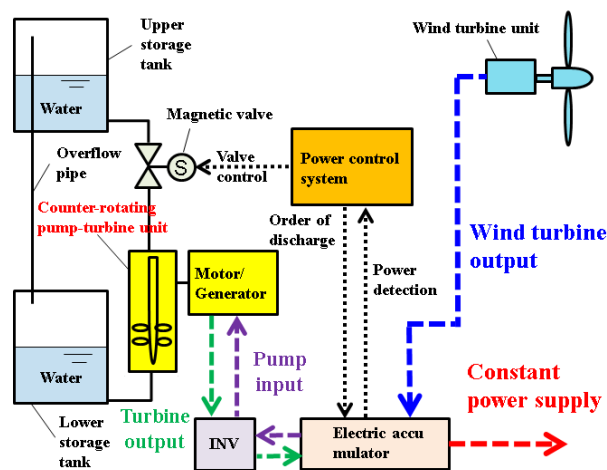
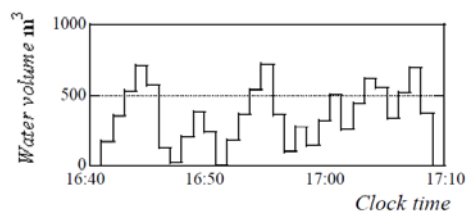
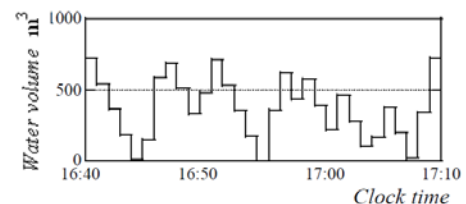


Fig. 3. Power stabilization system.



(a) Upper storage tank.



(b) Lower storage tank.

Fig. 4. Water volume in the storage tanks.

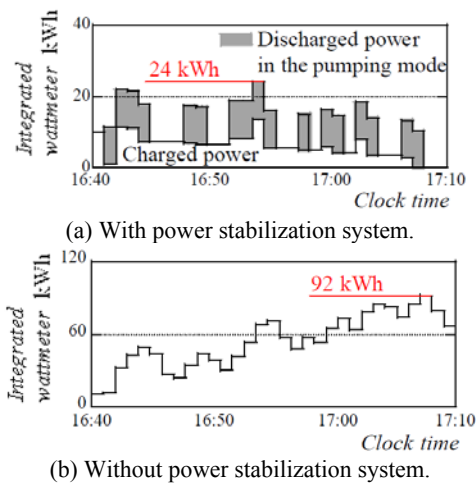


Fig. 5. Capacity in the electric accumulator.

### 3. Counter-Rotating Type Pump-Turbine Unit

#### 3.1 Model Unit

A counter-rotating type pump-turbine unit designed from the previous works [4] was considered for the optimization at its turbine mode in this work. The counter-rotating type pump-turbine unit (Fig. 6) consisted of a front impeller (rear runner) with five blades and a rear impeller (front runner) with four blades, and operated at a total speed of  $1,800 \text{ min}^{-1}$  in this work. In other words, the relative rotational speed between the front and rear runners was kept constant  $n_T = 1,800 \text{ min}^{-1}$  in this work. The blade sections were defined by NACA4409 hydrofoil with the single arc camber, and thereafter were redesigned numerically by using the commercial computational fluid dynamics (CFD) code to improve the pump performance [5]. The volumetric flow rate and unit output at the best efficiency point were  $0.025 \text{ m}^3/\text{s}$  and  $5.94 \text{ kW}$ , respectively, with the efficiency of 81.26%.

#### 3.2 Experiments

In this unit, a new type of the AC induction motor with the double rotational armatures has also been developed in place of the traditional type. The inner and the outer armatures drive the front and the rear impellers, respectively, while the relative rotational speed between both armatures is kept constant and that the rotational torque is counter-balanced between both impellers/armatures. Then, the angular momentum change through the front impeller must be the same as that through the rear impeller. Such operating conditions play important parts in adjusting automatically the front and the rear impeller works in response to the discharge, and then suppress successfully the unstable operation at the low discharge and the cavitation at the high discharge. Furthermore, the authors have also invented the counter-rotating type hydroelectric unit, which is composed of the tandem runners and the peculiar generator with double rotational armatures [6]. The unit has fruitful advantages that not only the induced voltage is sufficiently high without supplementary equipment such as a gearbox, but also the rotational moment hardly acts on the mounting bed because rotational torque counter-balances in armatures/runners.

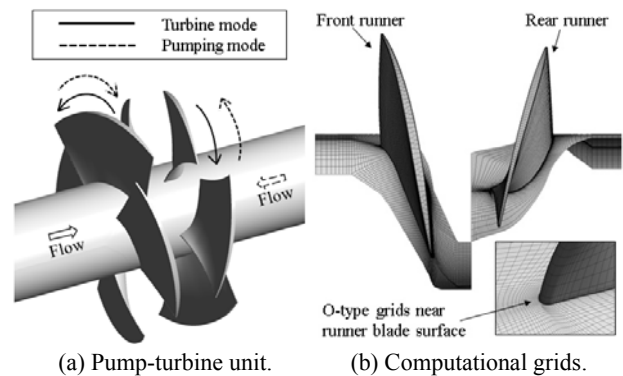


Fig. 6. Pump-turbine unit and computational grids.

#### 3.3 Numerical Simulation

The flow through the counter-rotating type pump-turbine unit was analyzed by solving three-dimensional incompressible RANS equations with a  $k-\omega$ -based shear stress transport (SST) turbulence model using a finite volume solver, the commercial code ANSYS CFX-12.1.

Figure 6(b) shows the computational domain for the numerical analysis, which consists of each single passage for both the rotational runners of the counter-rotating type pump-turbine unit. The flow between two adjacent runner blades was assumed to be periodic in the direction of rotation. The designed normal velocity and the averaged static pressure were set at the inlet and outlet of the computational domain, respectively. Water was considered as the working fluid. The solid surfaces in the computational domain were considered to be hydraulically smooth with adiabatic and no-slip conditions. The stage method [7] which performs a circumferential averaging of the fluxes through bands on the interface was used for the connection between the front and rear runners.

A hexahedral grid system was constructed in the computational domain with O-type grids near the blade surfaces and H/J/C/L-type grids in other regions, as shown in Fig. 6(b). The grid systems for the front and rear runner domains were constructed using approximately 510,000 and 420,000 grid points, respectively. Here, to benefit from the  $k-\omega$ -based SST model, the near-wall grid resolution was adjusted to keep  $y^+ \leq 2$  to accurately capture the wall shear stress and to implement the low-Reynolds-number SST model [7]. Consequentially, the total grid system has approximately 930,000 grid points for the numerical analysis.

As convergence criteria, the root-mean-square (RMS) values of the residuals of the governing equations were set to less than  $10^{-5}$  for all equations. The computations were conducted using an Intel Xeon CPU with a clock speed of 3.47 GHz. The converged solutions were obtained after 500 iterations and the computational time was approximately 4 hrs.

### 4. Turbine Performance

To verify the accuracy of the numerical analysis, the results of the flow analysis were compared to experimental data performed in the previous work [1].

The counter-rotating type pump-turbine unit used for this validation was considered as the reference model. Figure 7 shows the validation results in relation to the performance characteristic curves for the turbine output ( $P_{11} = P/D^2/H^{3/2}$ , where  $D$  means the diameter of turbine.) and efficiency at turbine mode of a unit. As shown in Fig. 7, the computed unit output and efficiency values are in reasonable agreement with the experimental data across the entire range of volume flow rates. Thus, it can be seen that the numerical method of this work is valid and reliable.

### 5. Blade Optimized at Turbine Mode

The aim of present optimization was to maximize the efficiency ( $\eta = P/\rho gQH$ , where  $P$ ,  $\rho$ ,  $g$ ,  $Q$ , and  $H$  denote the output power, density, acceleration of gravity, volume flow rate, and head.) at turbine mode of a counter-rotating type pump-turbine unit.

In the previous work [8], through analyses of the internal flow field at the best efficiency point of the reference model, some losses by the reverse flows were observed in the region of the near-hub of the both the runners. These losses have an adverse effect on the overall turbine performance of this unit. Hence, in order to reduce these losses, two design variables related to the hub profiles of both the runners were employed in this work. Namely angle  $\beta$  distribution at the hub span of both the runners was changed as shown in Fig. 8. Angle  $\beta$  is defined as the angle between the axis of rotation and a tangent of the camber line at the hub span. The entire  $\beta$  distribution changed equally along a runner hub having the fixed meridional geometry. Here, when the  $\beta$  distribution at each hub was changed equally, the runner blade profiles at other locations were interpolated using a B-spline curve from hub to tip, with the fixed vane profiles at the mid-span and tip.

To determine the feasible design space formed by ranges of the design variables, their sensitivity tests were carried out individually, and the ranges of the design variables were decided, as shown in Table I. Twelve design points were generated within the design space with the help of Latin hypercube sampling (LHS) [9] as a design-of-experiment. The objective functions for these design points were evaluated to construct the response surface for optimization.

The response surface approximation (RSA) [10] model was employed as the surrogate model to predict the objective function values in the design space determined by sensitivity tests. The RSA model, as a methodology of fitting a polynomial function to discrete responses obtained from numerical calculations, represents the association between design variables and response functions. The constructed response of a second-order polynomial RSA can be expressed as follows.

$$F(x) = C_0 + \sum_{j=1}^N C_j x_j + \sum_{j=1}^N C_{jj} x_j^2 + \sum_{i \neq j}^N C_{ij} x_i x_j \quad (1)$$

where  $C$ ,  $N$ , and  $x$  represent the regression analysis

coefficients, the number of design variables, and a set of design variables, respectively, and the number of regression analysis coefficients ( $C_0$ ,  $C_j$ , etc.) is  $(N + 1) \times (N + 2)/2$ . After constructing the RSA model, the optimum point was sought using sequential quadratic programming (SQP) [11] which is a gradient-based optimization technique and a generalization of Newton's method.

In the optimization, the RSA model for the objective function was obtained by using the numerical results at the twelve design points sampled by LHS. To measure the uncertainty in the set of coefficients of the polynomial for the RSA model, an analysis of variance (ANOVA) and a regression analysis with t-statistics [10]

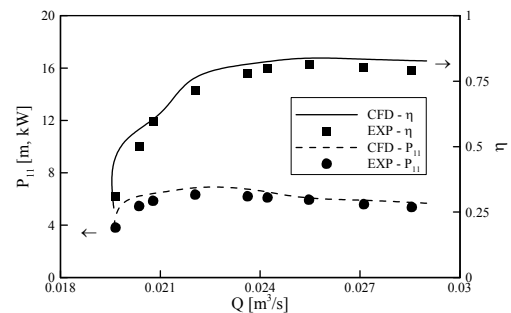


Fig. 7. Validation of the numerical results.

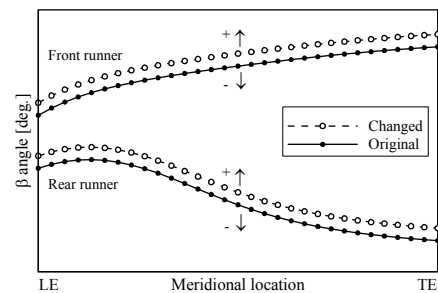


Fig. 8.  $\beta$  distribution at hub span of both runner blades.

Table I. - Ranges of design variables.

Variables	Lower	Reference	Upper
$\beta_F$	-6	0	2
$\beta_R$	-2	0	8

Table II. - Results of ANOVA and regression analysis.

Objective function	$R^2$	$R^2_{adj}$	RMSE
$\eta$	0.991	0.983	0.0003

Table III. - Results of the design optimization.  
(a) Design variables.

Designs	$\beta_F$ (deg.)	$\beta_R$ (deg.)
Reference	0	0
Optimum	-2.41	5.53

(b) Objective function values.

Designs	Prediction (%)	RANS (%)	Error (%)	Increment (%)
Reference	-	84.09	-	-
Optimum	86.76	86.77	0.01	2.68

were evaluated as shown in Table II. The values of  $R^2$  and  $R^2_{adj}$  for second-order curve fitting and the root mean square error (RMSE) of the RSA model are shown in Table II. Here,  $R^2$  and  $R^2_{adj}$  represent the correlation coefficient in the least squares surface fitting and the adjusted correlation coefficient, respectively. In Table II, the value of  $R^2_{adj}$  for the objective function is 0.983, and thus is reliable according to the  $0.9 < R^2_{adj} < 1.0$  range for accurate prediction of the RSA model [12]. Resultantly the constructed final RSA model can be expressed in terms of normalized design variables as follows.

$$\eta = 0.8589 + 0.0109x_1 + 0.00156x_2 + 0.0088x_1x_2 - 0.0142x_1^2 - 0.0151x_2^2 \quad (2)$$

where  $x_1$  and  $x_2$  indicate  $\beta_F$  and  $\beta_R$ , respectively.

The design variables for the optimized pump-turbine unit predicted by the RSA model are listed in Table III. In comparison with the reference model, the optimum design has smaller and bigger angles for the front and rear runners, respectively. The efficiency of the reference design obtained through the RANS analysis is 84.09%, as shown in Table III(b). On the other hand, the efficiency for the optimum design was predicted to be 86.76% based on the optimization, and was calculated to be 86.77% by the RANS analysis. The RSA model produced a good prediction with a relative error of 0.01%. Consequently, the efficiency of the optimum design represents a 2.68% improvement compared to the reference design at the best efficiency point.

Three-dimensional mesh plot of the constructed final RSA model is shown in Fig. 9. The optimum point located at (-2.41, 5.53) on the surface is clearly plotted in this figure. The sensitivity of the objective function to each design variable was tested, as shown in Fig. 10. The variation of each design variable was restricted to  $\pm 10\%$  of its optimum value.  $F_{opt}$  indicates the objective function's value at the optimum point, and shows that the objective function was more sensitive to the  $\beta_R$  than to the  $\beta_F$  near the optimum point.

To assess the performance characteristics of the optimized pump-turbine unit, flow analyses were carried out for several volume flow rates for the reference and optimum designs. Figure 11 shows the performance characteristic curves for the turbine output and efficiency at turbine mode of the reference and optimum designs. Considerable improvements in both the output and efficiency curves through optimization were observed for volume flow rates higher than about  $0.022 \text{ m}^3/\text{s}$ . It is noted that the optimum design shows especially the highest value in the region of high volume flow rates. As a result, by the present optimization, the output curve as well as the efficiency curve was also significantly improved in the high volume flow rate region.

Figure 12 shows the distribution of angle of attack at the root-mean-square radius, where the angle of attack was predicted with the averaging flow angle at 5 mm upstream and downstream sections of the runners, respectively. As shown in Fig. 12, the angles of attack for the front runners

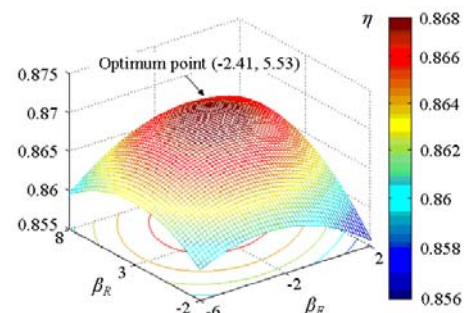


Fig. 9. Three-dimensional plot for the RSA model.

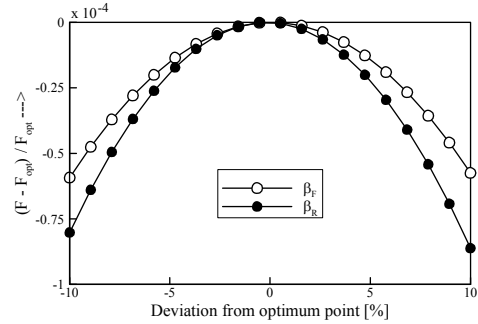


Fig. 10. Results of sensitivity test.

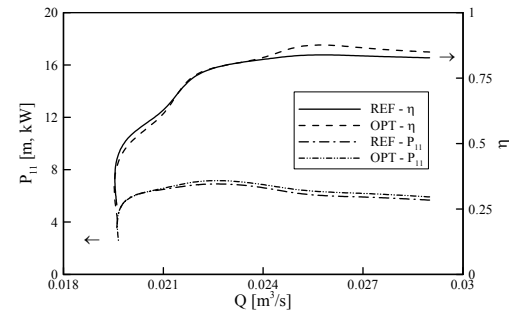


Fig. 11. Performance characteristic curves.

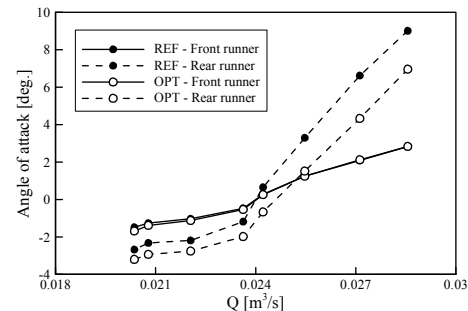
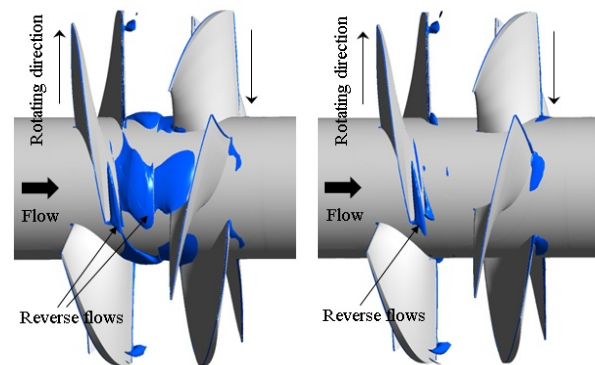


Fig. 12. Distribution of angle of attack at the root-mean-square radius.



(a) Reference design (b) Optimum design  
Fig. 13. Isosurfaces with reverse flow of 0.1 m/s.

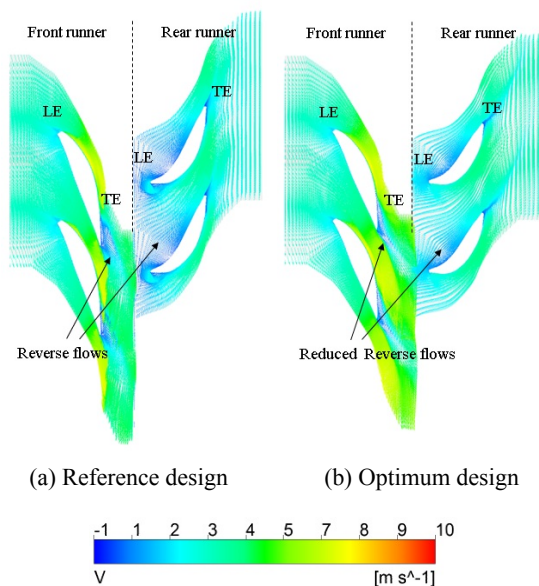


Fig. 14. Velocity vectors near hub span (unit: m/s).

of the reference and optimum designs are almost the same in the region of the entire range of volume flow rates, whereas the remarkable decrements of the angle of attack in the rear runner of the optimum design were occurred for the flow rate region higher than approximate  $0.023 \text{ m}^3/\text{s}$ . It can be seen that the reverse flow zone near hub in the rear runner of the optimum design was reduced clearly, and accordingly these results illustrate the enhancement of the pump-turbine unit's turbine performance as a result of the present optimization.

Figure 13 shows the isosurfaces having a reverse flow of  $0.1 \text{ m/s}$ . As mentioned already, this reverse flow as the negative velocity has an adverse effect on the overall turbine performance of a counter-rotating type pump-turbine unit. As shown in Fig. 13, an extensive reverse flow region formed on the hub between the both runners of the reference design, whereas a similar reverse flow isosurface disappeared clearly in the optimum design. On the other hand, small reverse flow components still occur near the downstream of 90% span in the front runners of both designs.

The velocity vectors near the hub span for the reference and optimum designs are plotted in Fig. 14. In the reference design, the reverse flow zone occurred on the suction side downstream of front runner. In particular, the extensive reverse flow occupying the entire blade-to-blade passage occurred on the upstream region of the reference rear runner. In contrast, the reverse flows were reduced generally in the optimum design, and above all the main flow was stabilized substantially at near upstream region of the rear runner. Therefore, it means that the optimum design produced mostly stable flows in the both runner passages.

## 6. Conclusion

The unique power stabilization system with the counter-rotating type pump-turbine unit was proposed to provide the constant power with high quality for the grid system.

The operation of the system was demonstrated in response to the fluctuating output from the wind turbine, and the counter-rotating type pump-turbine unit was proposed for the pumped storage. An optimization at turbine mode of this pump-turbine unit was also carried out to enhance the turbine efficiency of unit with two design variables related to the hub profiles for both the runners. The results of the design optimization showed that the efficiency for the optimum design was improved by 2.68% at the best efficiency point, and the efficiency curve was significantly enhanced in the region of high volume flow rates with the turbine output, as compared to the reference design. On the basis of the present results, the multi-objective optimization work for enhancing the performance at not only the turbine mode but also the pumping mode will be performed in the near future.

## References

- [1] Murakami, T., and Kanemoto, T., 2013, "Counter-Rotating Type Pump-Turbine Unit Cooperating with Wind Power Unit," *Journal of Thermal Science*, Vol. 22, No. 1, pp. 7-12.
- [2] Kanemoto, T., Kasahara, R., Honda, H., Miyaji, T., and Kim, J. H., 2013, "Counter-Rotating Type Pump-Turbine Unit Stabilizing Momentarily Fluctuating Power From Renewable Energy Resources," *Proceedings of ASME 2013 International Mechanical Engineering Congress & Exposition*, San Diego, California, USA, IMECE2013-66000, to be presented.
- [3] Kanemoto, T., and Oba, S., 2004, "Proposition of Unique Pumping System with Counter-Rotating Mechanism," *International Journal of Rotating Machinery*, Vol. 10, No. 4, pp. 233-240.
- [4] Kanemoto, T., Kimura, S., Oba, S., and Sato, M., 2000, "Smart Control of Axial Flow Pump Performances by Means of Counter-Rotating Type (1st Report, Counter-Rotating Type and Performances)," *Transaction of the JSME Series B*, Vol. 66, No. 651, pp. 2927-2933.
- [5] Oba, S., and Kanemoto, T., 2004, "Design of Counter-Rotating Impellers by Inverse Method to Improve Pump Performances," *22th IAHR Symposium on Hydraulic Machinery and Systems*, Stockholm, Sweden.
- [6] Tanaka, D., and Kanemoto, T., 2006, "Development of Counter-Rotational Type Machine for Hydroelectric Power generation (3<sup>rd</sup> Report, Design Materials for Solidity of Axial Flow Runners)," *Transaction of the JSME Series B*, Vol. 72, No. 715, pp. 686-692 (in Japanese).
- [7] ANSYS CFX-11.0, 2006, *ANSYS CFX-Solver Theory Guide*, ANSYS Inc.
- [8] Kasahara, R., Takano, G., Murakami, T., Kanemoto, T., and Komaki, K., 2012, "Counter-Rotating Type Axial Flow Pump Unit in Turbine Mode for Micro Grid System," *IOP Conference Series: Earth and Environmental Science*, Vol. 15, Paper 042026.
- [9] Sacks, J., Welch, W. J., Mitchell, T. J., and Wynn, H. P., 1989, "Design and Analysis of Computer Experiments," *Statistical Science*, Vol. 4, No. 4, pp. 409-435.
- [10] Myers, R. H., and Montgomery, D. C., 1995, *Response Surface Methodology: Process and Product Optimization Using Designed Experiments*, (Wiley, New York, USA).
- [11] MATLAB®, 2004, *The Language of Technical Computing*, Release 14, (The Math Work Inc).
- [12] Giunta, A. A., 1997, *Aircraft multidisciplinary design optimization using design of experimental theory and response surface modeling methods*, Ph.D. thesis, Department of Aerospace Engineering, Virginia Polytechnic Institute and State University, Blacksburg, VA.